

Dynamics of Charge-Resolved Entanglement after a Local Quench

Noa Feldman and Moshe Goldstein

Raymond and Beverly Sackler School of Physics and Astronomy, Tel-Aviv University, 6997801 Tel Aviv, Israel

Quantum entanglement and its main quantitative measures, the entanglement entropy and entanglement negativity, play a central role in many body physics. An interesting twist arises when the system considered has symmetries leading to conserved quantities: Recent studies introduced a way to define, represent in field theory, calculate for 1+1D conformal systems, and measure, the contribution of individual charge sectors to the entanglement measures between different parts of a system in its ground state. In this paper, we apply these ideas to the time evolution of the charge-resolved contributions to the entanglement entropy and negativity after a local quantum quench. We employ conformal field theory techniques, the time-dependent density matrix renormalization group algorithm, and exact solution in the noninteracting limit, finding good agreement between all these methods.

I. INTRODUCTION

The discussion of entanglement started in the early days of quantum mechanics by Einstein, Podolsky, and Rosen¹ as well as Schrödinger², yet quantum entanglement remains an active topic of research in several fields of quantum theory^{3–6}, and specifically in quantum many body systems^{7–9}. Entanglement in many body systems is used for elucidating their physics^{5,10–12}, for understanding the limits of simulating quantum systems on a classical computer^{13–16}, and to characterize their utility as a resource for various quantum information applications^{17–26}.

In order to define the entanglement measures we study in this paper, we introduce the density matrix (DM) for a state $|\psi\rangle$, $\rho = |\psi\rangle\langle\psi|$. We also define the reduced density matrix (RDM): For two subsystems A and B , and a pure state $|\psi\rangle$ of the combined subsystems, the RDM is defined to be $\rho_A = \text{Tr}_B \rho$. In this case (pure state of the total system), the basic measure for the entanglement of the subsystem A with its environment B is the *von Neumann entanglement entropy* (vNEE)²⁷:

$$S_A = -\text{Tr} \rho_A \log(\rho_A). \quad (1)$$

We also introduce the auxiliary *Rényi entropies*: The n th Rényi entropy (RE) is defined to be:

$$S_A^{(n)} = \text{Tr} \rho_A^n. \quad (2)$$

The REs obey $S_A = -\partial_n S_A^{(n)}|_{n \rightarrow 1}$. The REs are entanglement monotones, but they do not possess all the useful properties that the vNEE does²⁸. However, they are easier to calculate, and can be measured experimentally more easily^{29–40} (although a protocol for the measurement of the spectrum of the RDM of a bosonic system was proposed in Ref. 41).

When the total state of the two considered subsystems is not pure, different entanglement measures are needed. For two subsystems A_1 and A_2 , coupled to an environment B , a popular entanglement measure is the *entan-*

*glement negativity*⁴²:

$$\mathcal{N}_{A_1, A_2} = \frac{\left\| \rho_{A_1 \cup A_2}^{T_2} \right\| - 1}{2}, \quad (3)$$

where $\|\cdot\|$ denotes the trace norm, and the superscript T_2 stands for the partial transpose:

$$\begin{aligned} \rho_A &= \sum_{i,j,i',j'} c_{i,j,i',j'} |i\rangle_{A_1} |j\rangle_{A_2} \langle i'|_{A_1} \langle j'|_{A_2} \rightarrow \\ \rho_A^{T_2} &= \sum_{i,j,i',j'} c_{i,j,i',j'} |i\rangle_{A_1} |j'\rangle_{A_2} \langle i'|_{A_1} \langle j\rangle_{A_2}, \end{aligned}$$

where $(|i\rangle_{A_1}, |i'\rangle_{A_1})$ and $(|j\rangle_{A_2}, |j'\rangle_{A_2})$ are orthonormal bases for subsystems A_1 and A_2 respectively. Here too we define *Rényi negativities* (RNs):

$$\mathcal{N}_{A_1, A_2}^{(n)} = \text{Tr} \left(\rho_{A_1 \cup A_2}^{T_2} \right)^n, \quad (4)$$

which could be analytically continued from an even integer n to yield the negativity, using $\left\| \rho_{A_1 \cup A_2}^{T_2} \right\| = \lim_{n \rightarrow 1/2} \mathcal{N}_{A_1, A_2}^{(2n)}$. While the RNs are not even entanglement monotones (as opposed to the REs), they are still useful indicators of entanglement since (like the REs), they are experimentally measurable for both bosons^{43,44} and fermions⁴⁰, and are easier to calculate.

We study a system that has some conserved charge \hat{N} , that obeys $\hat{N}_A + \hat{N}_B = \hat{N}$, for \hat{N}_i the charge on subsystem i , such as a spin component or particle number. We assume that the state of the total system has some fixed value of \hat{N} , hence $[\rho, \hat{N}] = 0$. Performing a partial trace over the equation above, we get $[\rho_A, \hat{N}_A] = 0$. This implies that the RDM is block diagonal, each block corresponding to some eigenvalue of \hat{N}_A and denoted by $\rho_A^{(N_A)}$. This allows to define the *charge resolved* vNEE and REs^{45–49}:

$$\begin{aligned} S_A(N_A) &= -\text{Tr} \rho_A^{(N_A)} \log \rho_A^{(N_A)}, \\ S_A^{(n)}(N_A) &= \text{Tr} \left(\rho_A^{(N_A)} \right)^n. \end{aligned} \quad (5)$$

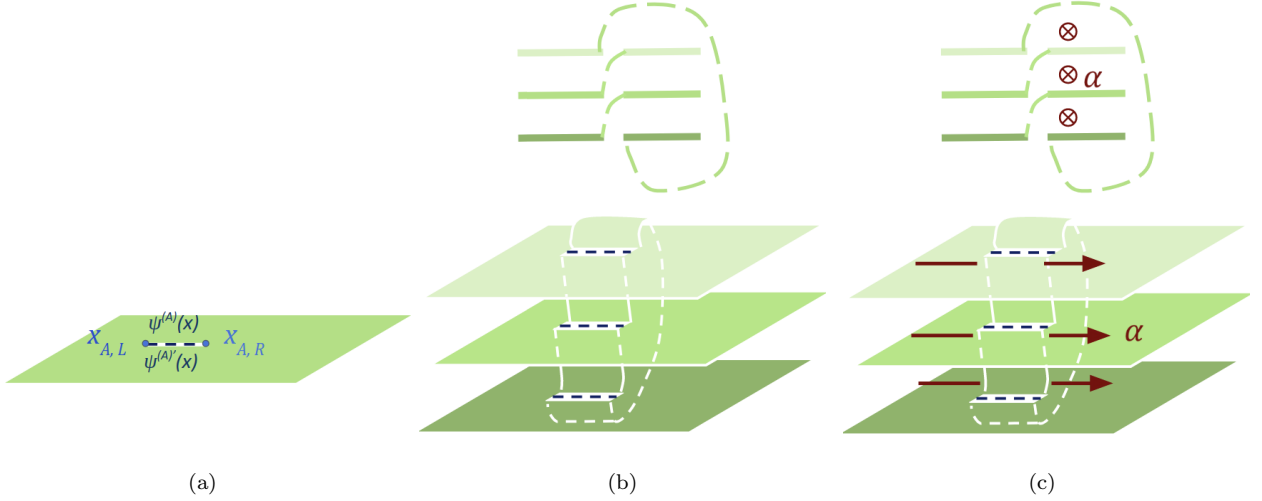


FIG. 1. (a) Geometric representation of the RDM matrix element $\langle \psi^{(A)}(x) | \rho_A | \psi^{(A)'}(x) \rangle$ as an infinite Riemann sheet with a slit corresponding to subsystem A , with the indicated boundary conditions on the fields. (b) Side and Front view of the geometric representation of the Rényi entropy as a complex manifold composed of several copies of the RDM. (c) Inserting an AB-flux α coupled to the charge \hat{N} between the Riemann sheets. Particles living on subsystem A will acquire a phase α , while particles living on the environment will not be affected by the flux, resulting in a phase $\hat{N}_A \alpha$ acquired by the system.

For the case of two subsystems coupled to an environment, it is useful to define the charge imbalance: $\hat{Q} = \hat{N}_{A_1} - \hat{N}_{A_2}^{T_2}$, since by simple algebra it can be shown that $[\rho_A^{T_2}, Q] = 0$. Note that in a general Fock space, $\hat{N}_{A_2}^{T_2} = \hat{N}_{A_2}$. We may then define the *charge imbalance resolved negativity* and RNs⁴³:

$$\mathcal{N}(Q) = \frac{\left| \left(\rho_A^{T_2} \right)^{(Q)} \right| - 1}{2}, \quad (6)$$

$$\mathcal{N}_{A_1, A_2}^{(n)}(Q) = \text{Tr} \left(\left(\rho_A^{T_2} \right)^{(Q)} \right)^n.$$

By definition, $S_A^{(1)}(N_A)$ is the charge distribution in subsystem A , and $\mathcal{N}_{A_1, A_2}^{(1)}(Q)$ is the charge imbalance distribution, demonstrating an inherent relation between entanglement and charge distribution. The charge resolved entanglement can be used as an instrument to study entanglement properties and gain a better understanding of the charge block structure of the entanglement spectrum. A particular interest in the relation between charge distribution and entanglement has risen for systems after a local quench: We prepare two subsystems A and B in the ground state, couple the two subsystems at $t = 0$ and study the evolution of entanglement between them. In Ref. 50 a relation between charge distribution (quantum noise) and the entanglement has been derived for noninteracting fermions undergoing this type of quench, and motivated further study of the relation between entanglement and charge distribution^{51–64}. With the charge-resolved entanglement mea-

sures just discussed it becomes apparent that one should not separately address the dynamics of charge and entanglement, but rather their combined measures. The goal of this work is to address this question.

In this paper we combine the methods from Refs. 43 and 46 for calculating the time dependent charge-resolved entanglement in 1+1D conformal field theory (CFT) systems. We compare them to exact results for the XX model, as well as to time dependent density matrix renormalization group (tDMRG) results for the XXZ model [Eq. (29)]. We get satisfying results for the dynamics of the charge resolved vNEE. As for the charge imbalance resolved negativity, the CFT results involve hard-to-calculate conformal blocks, but we can still derive approximate expressions which qualitatively match the numerical results.

The rest of the paper is organized as follows: In Sec. II we present the theoretical background for the calculation of entanglement entropies and negativities for 1+1D CFT, and extend this method for calculating the charge resolved entanglement entropies and charge imbalance resolved negativities. We then use this method to calculate the charge resolved vNEEs and imbalance resolved RNs after a local quench. In Sec. III we compare the CFT predictions to numerical results for the XX and XXZ model. We summarize our findings and outline future directions in Sec. IV.

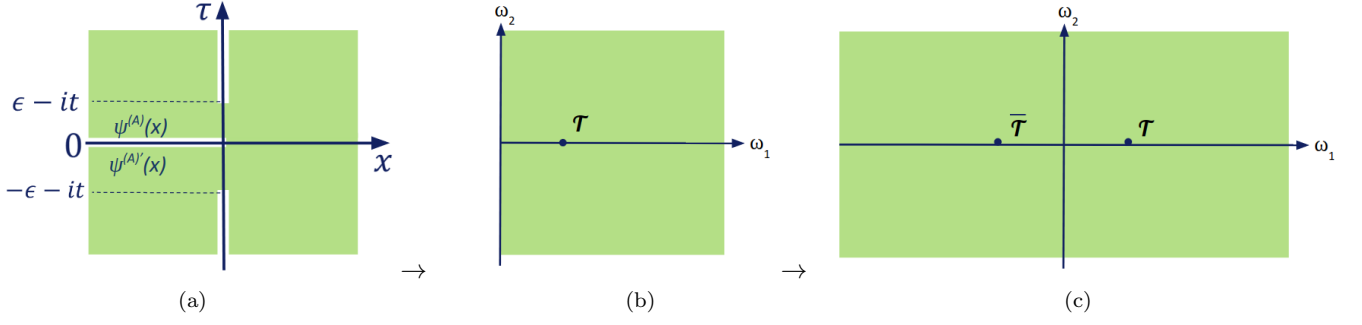


FIG. 2. (a) A geometrical representation of the time dependent RDM element after a local quantum quench. A twist field operator can be added to simulate the replica trick. (b) We map the cut plane from (a) to the right half plane using the conformal transformation (10). (c) “Unfolding” of the system from the right half plane to the full plane, doubling the number of operators.

II. CONFORMAL FIELD THEORY ANALYSIS

A. The Entanglement Entropy

We will first recap the calculation of the total REs of a 1+1D CFT in the ground state and after a local quench⁵, and then show how to generalize these techniques to the charge-resolved REs. The calculation is based on the replica trick. Space-imaginary time will be represented by the complex plane, with $z = x + iv\tau$, with v the velocity of excitations. Representing the DM as a path integral, the RDM (when the total system is in its ground state) is represented as a path integral over the complex plane with a cut at $\tau = 0$ at subsystem A ’s coordinates, different boundary conditions on which giving different matrix elements of the RDM, see Fig 1a. Sewing n copies of the RDM together one obtains the n th RE as a path integral on an n -sheet Riemann surface, see Fig. 1b. The transition between the copies is effected by *twist field operators* \mathcal{T}_n and $\tilde{\mathcal{T}}_n$. \mathcal{T}_n and $\tilde{\mathcal{T}}_n$ transfer particles from one copy to the next clockwise and counterclockwise, respectively. Hence, the RE is proportional to the correlation function of these twist fields:

$$S_A^{(n)} \propto \left\langle \mathcal{T}_n(x = x_{A,L}, \tau = 0) \tilde{\mathcal{T}}_n(x = x_{A,R}, \tau = 0) \right\rangle, \quad (7)$$

for $x = x_{A,L}$ and $x = x_{A,R}$ the ends of subsystem A (taken as a single interval). The scaling dimension of the twist fields is:

$$d_n = \bar{d}_n = \frac{c}{24} (n - n^{-1}), \quad (8)$$

and the resulting RE and vNEE are:

$$S_A^{(n)} = \text{Tr} \rho_A^n = c_n \left(\frac{L_A}{a} \right)^{-c(n - n^{-1})/6}, \quad (9)$$

$$S_A = \frac{c}{3} \log \frac{L_A}{a} + c'_1,$$

where $L_A = |x_{A,L} - x_{A,R}|$ is the length of subsystem A , a is a cutoff corresponding to, e.g., a lattice spacing, c is the conformal central charge, and c_n and c'_1 are constants that cannot be predicted using CFT.

Let us now go on to the time-dependent local quench scenario. We prepare two identical systems in the ground state, and at time $t = 0$ we couple them at one contact point. For this time dependent case, the geometry representing the RDM is slightly more complicated: The two halves of the system are not connected before $t = 0$. Upon analytical continuation to imaginary time, this is expressed as slits in each sheet, parallel to the imaginary time axis. The slits are separated by a small gap ϵ , which serves as a convergence factor. This is shown in Fig. 2a. We then use the conformal transformation⁵:

$$\omega(z) = \frac{z}{\epsilon} + \sqrt{\left(\frac{z}{\epsilon}\right)^2 + 1}, \quad (10)$$

which takes the Riemann sheet with the slits into the right half plane, as demonstrated in Fig. 2b.

A system living on the right half plane has a boundary on the imaginary time axis, and requires the use of boundary CFT (BCFT)⁶⁵: We separate our field into a holomorphic part and an anti-holomorphic part, and “unfold” the anti-holomorphic part into the left half plane. This also duplicates the operators in our system, turning an n -point function into a $2n$ -point function, as demonstrated in Fig. 2c. For an infinite system with one boundary point between the systems A and B we are then left with a two-point function for the composite twist fields. The final result for the entanglement when A and B are the two parts of the system brought together by the local quench, is:

$$S_A^{(n)}(t) \propto \left(\frac{\epsilon^2 + (vt)^2}{a\epsilon/2} \right)^{-c(n - n^{-1})/12}, \quad (11)$$

$$S_A(t) = \frac{c}{3} \log \frac{vt}{a} + k_0,$$

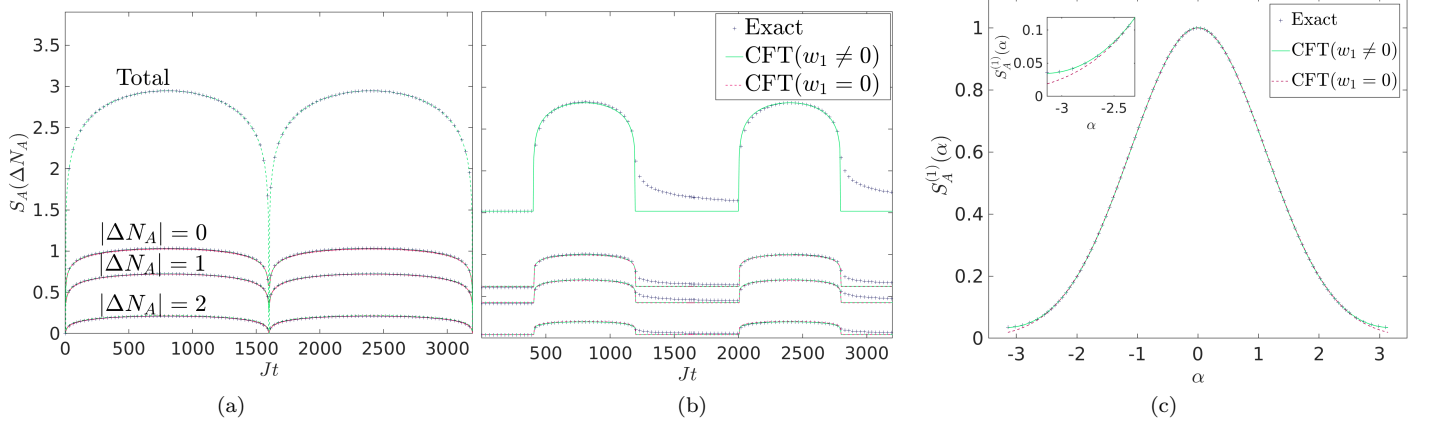


FIG. 3. Exact results for the charge resolved entanglement of the XX model with site number $L/a = 3200$ sites. In (a) the boundary between the subsystems A and B is the quench point, and in (b) the boundary is shifted by $L/4a$ from the quench point. In (c) we present the fit of the flux resolved 1st RE for some generic $Jt = 195$. Inset: Zoom-in on the region in which the difference between the results for $w_1 = 0$ and $w_1 \neq 0$ (defined in Eq. (19)) is noticeable for α close to $-\pi$.

where the last equation applies for $vt \gg \epsilon$, and k_0 a non-universal constant.

For finite subsystems $L_A = L_B = L/2$, one may use the following conformal transformation⁶⁶:

$$\omega(z) = \coth\left(\frac{\pi\epsilon}{2L}\right) \frac{1 + \zeta(z)}{1 - \zeta(z)}, \quad (12)$$

$$\text{with } \zeta(z) = \sqrt{\frac{\sinh \frac{\pi}{L}(z + \epsilon)}{\sinh \frac{\pi}{L}(z - \epsilon)}}.$$

Let us now move to the calculation of the charge-resolved entropy in the ground state. In Ref. 46, the twist fields are multiplied by a vertex operator $\mathcal{V}(\alpha)$. For a charge \hat{N} related to an abelian $U(1)$ symmetry, the vertex operator is coupled to the charge such that a particle going around $\mathcal{V}(\alpha)$ will acquire a phase $e^{i\alpha}$. If the vertex operators are placed at the edges of subsystem A , as the twist fields are, the resulting correlation function will give:

$$S_A^{(n)}(\alpha) = \text{Tr} \rho_A^n e^{i\hat{N}_A \alpha}. \quad (13)$$

We can think of this vertex operator as introducing a flux α for the particles, and define the measure in (13) to be the *flux resolved RE*, see Fig. 1c. A Fourier transform will lead us to the charge resolved RE,

$$S_A^{(n)}(N_A) = \int_{-\pi}^{\pi} \frac{d\alpha}{2\pi} e^{-iN_A \alpha} S_A^{(n)}(\alpha). \quad (14)$$

For a gapless interacting fermionic system described as a Luttinger liquid^{67,68} living on the j th copy with a bosonic field ϕ_j , the vertex operator can be chosen as

$$\mathcal{V} = e^{i\frac{\alpha}{2\pi}\phi_j}, \quad (15)$$

with a scaling dimension

$$d^{(\mathcal{V})} = \frac{K}{2} \left(\frac{\alpha^2}{2\pi} \right), \quad (16)$$

where K is the Luttinger parameter ($K < 1$, $K > 1$, and $K = 1$ corresponding, respectively, to repulsive, attractive, or no interaction between the fermions).

One may now derive an expression for the scaling function of the composite twist field⁴⁶:

$$d_n(\alpha) = \frac{c(n - n^{-1})}{24} + \frac{d^{(\mathcal{V})}}{n}. \quad (17)$$

This leads to Gaussian dependence of the charge-resolved RE on the charge, provided $\ln(L_A/a) \gg 1$:

$$S_A^{(n)}(N_A) \cong S_A^{(n)}(\alpha = 0) \sqrt{\frac{\pi n}{2K \ln L_A/a}} e^{-\frac{\pi^2 n \Delta N_A^2}{2K \ln L_A/a}}, \quad (18)$$

where $\Delta N_A = N_A - \langle \hat{N}_A \rangle$, $\langle \hat{N}_A \rangle$ being the expectation value of \hat{N}_A in the ground state.

These results could be extended to smaller subsystems. We notice that the most general form for \mathcal{V} is in fact:

$$\mathcal{V} = \sum_{m=-\infty}^{\infty} w_{|m|} e^{i\left(\frac{\alpha + 2\pi m}{2\pi}\right)^2 \phi}, \quad (19)$$

where m is integer and $w_{|m|}$ is the corresponding weight. For a large enough L_A , the zeroth order term ($w_{|m|} = 0$ for $m \neq 0$) is sufficient, since its correlation function features the slowest decay with subsystem size. In the time dependent case (to be discussed shortly), we often find it necessary to include the next order $w_1 \neq 0$, since its contribution is becoming important for short times. For the XX model studied below, the parameter w_1 can be

extracted for the ground state using similar methods to those employed in Ref. 69. However, in the time dependent case no such results are available, and we resort to extracting w_1 from a fit to our numerical results.

Having laid out all the necessary groundwork, we may now derive our new results for the charge resolved entropies following a local quench. Combining Eqs. (11), (16) and (19), we find the following expression for the dynamics of the flux resolved RE after a local quench:

$$S_A^{(n)}(\alpha, t) = S_A^{(n)}(\alpha = 0, t) \times \sum_{m=-\infty}^{\infty} w_m \left(\frac{(vt)^2 + \epsilon^2}{a\epsilon/2} \right)^{-\frac{c}{12}(n-n^{-1}) - \frac{K}{n} \left(\frac{\alpha + 2\pi m}{2\pi} \right)^2} \quad (20)$$

Plugging this into Eq. (14) will give us the charge resolved RE. For a finite system as studied below, we use the transformation (12) and get a prediction similar to (20). For the case where the boundary between subsystems A and B is moved from the quench point, we use the same conformal transformation (12), but place the twist fields away from the slits⁶⁶. We do not write the results explicitly here since they are too cumbersome.

B. The Entanglement Negativity

The replica trick for the negativity is derived in Ref. 70. For two adjacent single-interval subsystems $A_1 = [x_{A_1,L}, x_{A_1,R}]$, $A_2 = [x_{A_1,R}, x_{A_2,R}]$, twist field operators are added at the three boundary points $x_{A_1,L}, x_{A_1,R}, x_{A_2,R}$ such that:

$$\mathcal{N}_{A_1,A_2}^{(n)} \propto \left\langle \mathcal{T}_n(x_{A_1,L}, 0) \tilde{\mathcal{T}}_n^2(x_{A_1,R}, 0) \mathcal{T}_n(x_{A_2,R}, 0) \right\rangle. \quad (21)$$

Calculating the negativity for the local quench case, we are again forced to use BCFT and double the number of operators. We are left with calculating a 6-point function. For a j -point function with $j \geq 4$, the result can be predicted by CFT only up to a nonuniversal function \mathcal{F}^{71} , which depends on the full operators content of the studied theory. We thus restrict ourselves to limits in which \mathcal{F} is approximately constant. It is for this reason that we do not study the case where A_1 and A_2 are disjoint — following the arguments above, we will need to calculate an 8-point function, for which the effect of nonuniversal function \mathcal{F} is expected to be even more significant.

In Ref. 72 the RN after a local quench was found to be:

$$\mathcal{N}_{A_1,A_2}^{(n)} = \prod_i \left| \frac{d\omega}{dz} \right|_{z_i}^{d_i} \langle \mathcal{T}_n(\omega_1) \tilde{\mathcal{T}}_n^2(\omega_2) \mathcal{T}_n(\omega_3) \rangle, \quad (22)$$

where ω is defined in Eq. (10) or (12). The unfolded

6-point function was found to be:

$$\langle \mathcal{T}_n(\omega_1) \tilde{\mathcal{T}}_n^2(\omega_2) \mathcal{T}_n(\omega_3) \rangle = \prod_i \frac{1}{|\omega_i - \tilde{\omega}_i|^{d_{n,i}}} \left(\frac{\eta_{1,3}^{d_n^{(2)} - 2d_n}}{\eta_{1,2}^{d_n^{(2)}} \eta_{2,3}^{d_n^{(2)}}} \right)^{1/2} \mathcal{F}(\{\eta_{j,k}\}), \quad (23)$$

where $d_n^{(2)}$ is the scaling dimension of \mathcal{T}_n^2 calculated in Ref. 70, $\tilde{\omega}_i = -\omega_i^*$, $\eta_{i,j} = \frac{(\omega_i - \omega_j)(\tilde{\omega}_i - \tilde{\omega}_j)}{(\tilde{\omega}_i - \omega_j)(\omega_i - \tilde{\omega}_j)}$, and $d_{n,i} = d_n$ for $i = 1, 3$ and $d_{n,i} = d_n^{(2)}$ for $i = 2$. \mathcal{F} approaches a constant value for $vt \ll l$, $vt = l + 0^+$, and $vt > l$ for two identical subsystems $L_{A_1} = L_{A_2} = l$, which is the case on which we focus here. We will only consider $l \ll L$, and so neglect corrections due to boundary conditions.

The charge-imbalance resolved RNs are again obtained from the flux resolved RNs,

$$\mathcal{N}_{A_1,A_2}^{(n)}(\alpha) = \text{Tr}((\rho_A^{T_2})^n e^{i\hat{Q}\alpha}), \quad (24)$$

$$\mathcal{N}_{A_1,A_2}^{(n)}(Q) = \int_{-\pi}^{\pi} \frac{d\alpha}{2\pi} \mathcal{N}_{A_1,A_2}^{(n)}(\alpha) e^{-i\alpha Q}. \quad (25)$$

We obtain the flux resolved RNs by adding vertex operators at the boundaries between the subsystems⁴³. The additivity of the scaling dimensions, Eq. (17), results in

$$\frac{\mathcal{N}_{A_1,A_2}^{(n)}(\alpha)}{\mathcal{N}_{A_1,A_2}^{(n)}} \propto \langle \mathcal{V}(\alpha, x_{A_1,L}, 0) \mathcal{V}(-2\alpha, x_{A_1,R}, 0) \mathcal{V}(\alpha, x_{A_2,R}, 0) \rangle. \quad (26)$$

We can now present our new results. Combining Eqs. (10) and (26), and using the vertex operators correlation function from Ref. 71, we obtain the flux resolved RN for two adjacent systems with an infinite environment (we present the expression for the simple case, $w_{|m|>0} = 0$)

$$\frac{\mathcal{N}_{A_1,A_2}^{(n)}(\alpha, t)}{\mathcal{N}_{A_1,A_2}^{(n)}(t)} = \prod_{i,j} e^{-\frac{\alpha_i \alpha_j}{(2\pi)^2} \ln(\omega'_i - \omega'_j)}, \quad (27)$$

where $i, j = 1 \dots 6$ count the 6 positions of the vertex operators, $\omega'_i = \omega_1, \omega_2, \omega_3, \tilde{\omega}_1, \tilde{\omega}_2, \tilde{\omega}_3$ and $\alpha_i = \alpha, -2\alpha, \alpha, -\alpha, 2\alpha, -\alpha$, respectively. For the first order in α (taking $w_m \neq 0$ for $m = \pm 1$ in Eq. (19)), we get

$$\frac{\mathcal{N}_{A_1,A_2}^{(n)}(\alpha, t)}{\mathcal{N}_{A_1,A_2}^{(n)}(t)} = \sum_{\mu} \prod_{i,j} e^{-\frac{\alpha_i^{(\mu)} \alpha_j^{(\mu)}}{(2\pi)^2} \ln(\omega'_i - \omega'_j)}, \quad (28)$$

where $\mu = 1 \dots 6$, and $\alpha_i^{(\mu)} = \alpha_i + 2\pi\delta_{i,\mu} - 2\pi\delta_{i+3,\mu}$.

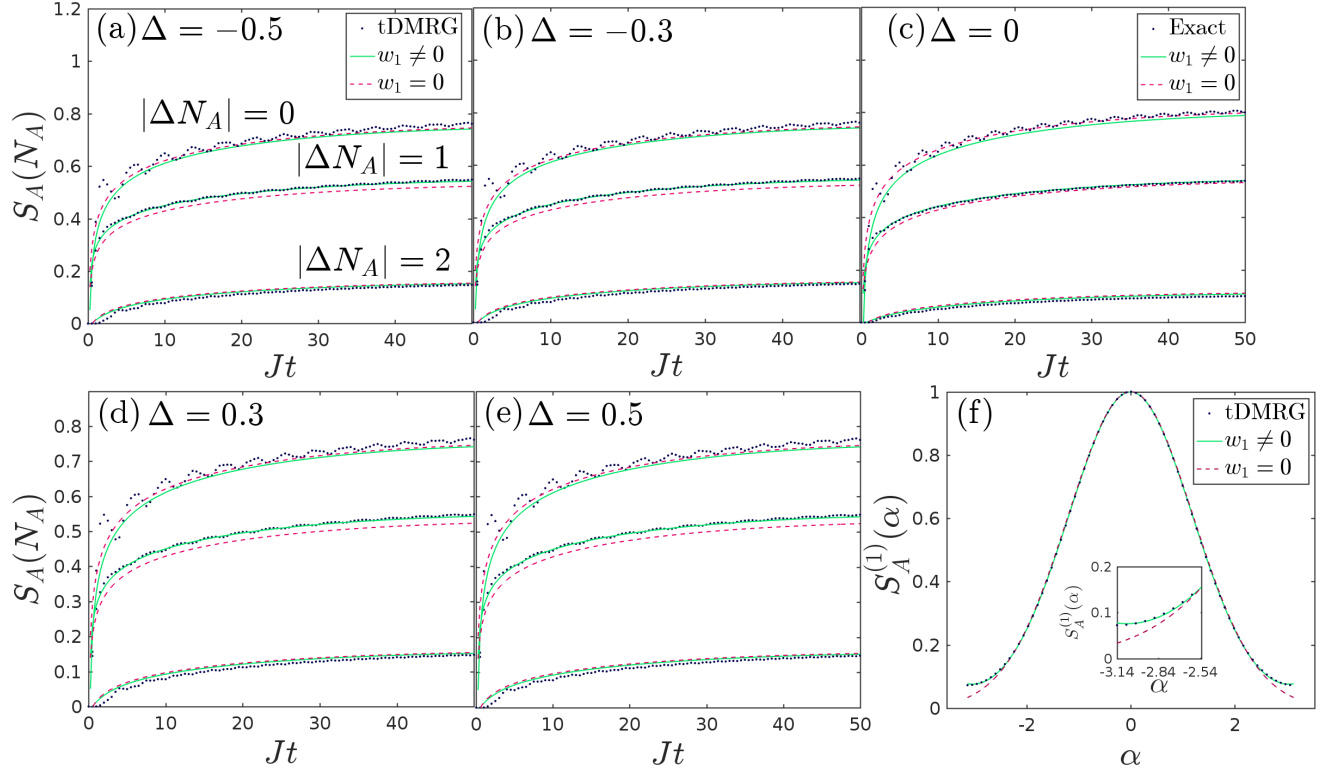


FIG. 4. (a, b, d, e) tDMRG results for the charge-resolved entanglement of the XXZ model with different values of Δ , for a system with $L/a = 256$ sites. For comparison, exact diagonalization results for a system of the same size in the XX model are presented in (c). In (f) we present the fit of the flux resolved 1st RE for a generic time $Jt = 26$. Inset: Zoom-in on the region near $\alpha = -\pi$.

III. NUMERICAL RESULTS

A. Entanglement Entropy

The XXZ model. We compare our CFT predictions to numerically obtained results for the XXZ spin chain,

$$H = J \sum_n (\sigma_n^+ \sigma_{n+1}^- + \text{h.c.} + \Delta \sigma_n^z \sigma_{n+1}^z), \quad (29)$$

when σ^+ , σ^- , σ^z are the Pauli matrices. Using the Jordan Wigner transformation⁷³

$$\begin{aligned} \sigma_i^+ &= f_i^\dagger, \\ \sigma_i^- &= f_i, \\ \sigma_i^z &= 2f_i^\dagger f_i - 1, \\ c_i &= e^{-i\pi \sum_{j<i} f_j^\dagger f_j} f_i, \end{aligned} \quad (30)$$

the XXZ model can be interpreted as a spinless fermionic chain.

$$H = J \sum_n \left(c_n^\dagger c_{n+1} + \text{h.c.} + \Delta (2c_n^\dagger c_n - 1)(2c_{n+1}^\dagger c_{n+1} - 1) \right), \quad (31)$$

where the c_n annihilation operators obey the fermionic anti-commutation relations. The system is a gapless Luttinger liquid for $-1 < \Delta \leq 1$. Its Luttinger parameter and velocity can be extracted from the Bethe ansatz⁷⁴,

$$\begin{aligned} K &= \frac{\pi}{2(\pi - \arccos \Delta)}, \\ v &= \frac{2v_F (\pi - \arccos \Delta)}{\pi}. \end{aligned} \quad (32)$$

We note that for lower values of Δ , corresponding to higher values of K , the Gaussian distribution of the charge resolved entanglement is expected to be wider, and the effect of higher orders of α smaller, as can be seen from Eq. (20).

For $\Delta = 0$ Eq. (31) describes spinless noninteracting fermions, allowing an exact calculation of the entanglement. Then, the entanglement Hamiltonian \hat{H}_A , defined

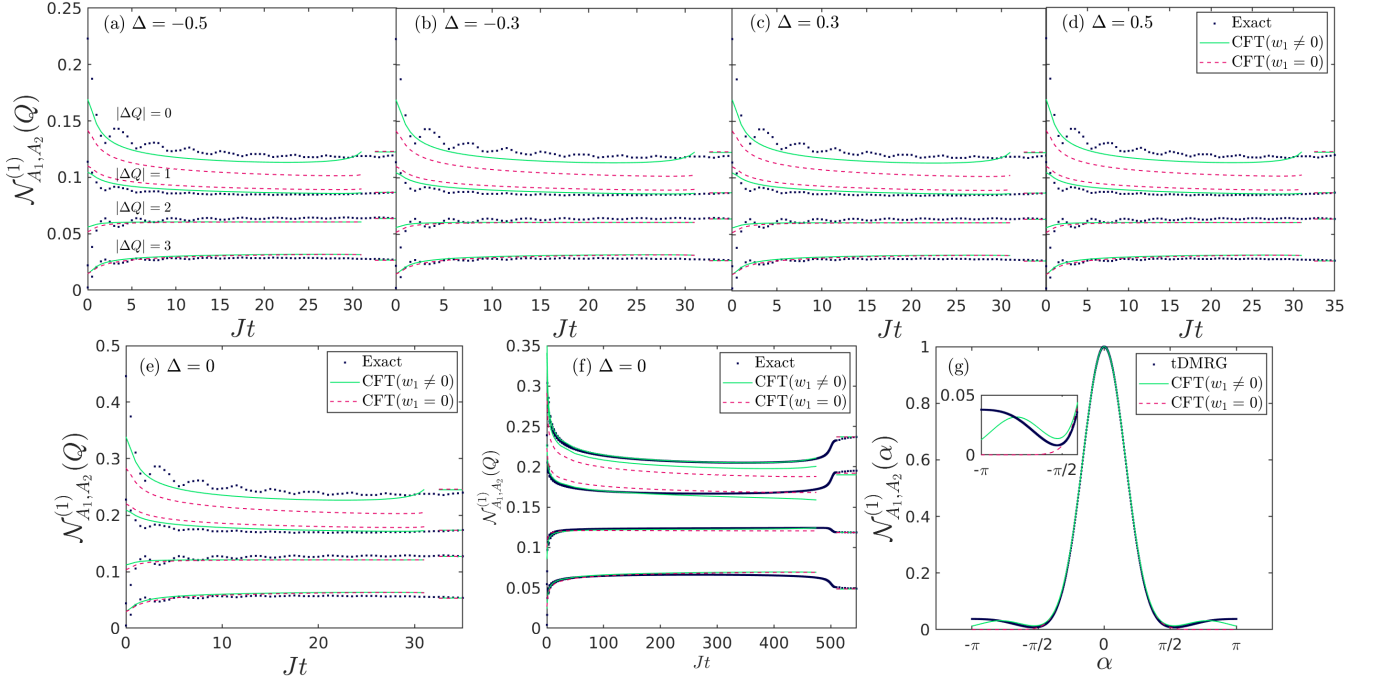


FIG. 5. The first imbalance resolved RN. (a-d) tDMRG results for the XXZ model with different values of Δ for $\frac{L}{a} = 256$ and $\frac{L_{A_i}}{a} = 64$. (e) Exact results for a system with the same size as the tDMRG results for comparison. (f) The exactly solvable XX model for a very large system ($\frac{L}{a} = 10,000$), for $\frac{L_{A_i}}{a} = 1000$. For $t \approx \frac{L_{A_i}}{v}$ the conformal approximation is not applicable, and these region were omitted. (g) A fit of the flux resolved first RN for for some generic $Jt = 6$ for the XXZ model with $\Delta = -0.5$. Inset: Zoom-in on the region near $\alpha = -\pi$.

as $\rho_A = e^{-\hat{H}_A}$, is quadratic. We follow Ref. 46 (based on the method introduced in Ref. 75), and obtain exact results for the entanglement entropies,

$$S_A^{(n)} = \prod_n [e^{i\alpha}(f_l)^n + (1 - f_l)^n], \quad (33)$$

where $f_l = 1/(e^{\epsilon_l} + 1)$, and ϵ_l are the eigenvalues of \hat{H}_A . f_l are the eigenvalues of the subsystem correlation matrix $C_{ij} = \langle c_i^\dagger c_j \rangle$, $i, j = 1 \dots L_A$, which can be obtained exactly for the noninteracting case.

Results for the case in which the boundary point between A and B is the quench point are presented in Fig. 3a, and for the case when the boundary point is moved away by $x = l$ from the quench point in Fig. 3b. We use open boundary conditions throughout. In all cases in this study, a and w_1 from Eq. (20) were used as fitting parameters. The entanglement is periodic in time, as predicted by Eq. (12). This is the result of the entanglement being carried by quasiparticles moving in velocity v , bumping the ends of the system and coming back to the other side⁶⁶. In Fig. 3b, CFT predicts the entanglement to be constant for $\text{mod}(vt, L) < l$ or $\text{mod}(vt, L) > L - l$, when these quasiparticles are allegedly outside of subsystem A . The exact results present some tails in these time regimes, which are caused by excitations moving in a slower velocity than v , which are not accounted for by

CFT⁶⁶. We present results both for the zeroth order case, calculated from Eq. (20) with $w_m = 0$ for $m \neq 0$, and for the first order, in which $w_1 \neq 0$. The zeroth order seems to be a satisfying approximation from Figs. 3a and 3b, but as can be seen in Fig. 3c, it is insufficient for large values of $|\alpha|$.

For nonzero values of Δ , we compare the CFT prediction to numerical results obtained by the tDMRG algorithm^{15,76–79}, employing the QSpace tensor library⁸⁰. The bond dimension was set to 1,024 and the truncation error to 10^{-8} in all tDMRG runs for the entanglement entropy (in practice the truncation error was 10^{-10} or less). We used a second order Trotter approximation with a timestep of $\Delta t = 10^{-2}J^{-1}$. The extraction of the charged resolved entanglement spectrum is natural in this method, thanks to the block diagonal form of the MPS matrices. In order to stay well within the CFT region, we chose $-0.5 \leq \Delta \leq 0.5$. Results for several values of Δ for open boundary conditions are plotted in Fig. 4. Here too results for both $w_1 = 0$ and $w_1 \neq 0$ are presented. $w_1 = 0$ appears to be generally a satisfactory fit, as in the noninteracting case. We see oscillations in the numerical data not predicted by CFT: These are oscillations due to finite lattice spacing, which are absent in the CFT approximation and decrease for large t (which is why they were not seen in Fig. 3, where the system length and achievable timescales are much longer). We note that the contribution of the corresponding spatial oscillations

was calculated for the ground state case of the XX model in Ref. 69, but these results are not straightforward to extend to the current time-dependent case.

B. Entanglement Negativity

The numerical method for the exactly solvable XX model is developed in Ref. 43 and based on the fact that the partially transposed RDM is a sum of two Gaussian matrices^{81,82}: $\rho_A^{T_2} = \sum_{\sigma=\pm 1} u_{\sigma} \frac{\hat{O}_{\sigma}}{\text{Tr} \hat{O}_{\sigma}}$, where u_{σ} are coefficients and $\hat{O}_{\sigma} = e^{\sum_{ij} c_i^{\dagger} W_{ij}^{(\sigma)} c_j}$, where the matrices $W_{ij}^{(\sigma)}$ can be extracted from the correlation matrix C_{ij} defined in the previous Subsection. In Ref. 43 it was shown that for a quadratic operator $\hat{X} = \sum_{ij} c_i^{\dagger} X_{ij} c_j$ (such as the charge imbalance \hat{Q}),

$$\text{Tr} \left[e^{i\hat{X}} \left(\rho_A^{T_2} \right)^n \right] = \sum_{\{\sigma\}} u_{\{\sigma\}} \det \left(\frac{1 + e^X \prod_i e^{W^{(\sigma_i)}}}{\prod_i (1 + e^{W^{(\sigma_i)}})} \right), \quad (34)$$

where $u_{\{\sigma\}} = \prod_i u_{\sigma_i}$. Combining the equation above with Eq. (24), which is of the form of the RHS of Eq. (34), we can obtain the exact RNs for the XX model.

In this method, the only RNs that are numerically accessible are $\mathcal{N}_{A_1, A_2}^{(1)}$, $\mathcal{N}_{A_1, A_2}^{(2)}$, and $\mathcal{N}_{A_1, A_2}^{(3)}$, since the matrices in the denominator in Eq. (34) are almost singular, and only for $n \leq 3$ one can explicitly cancel the small denominator against a corresponding factor in the numerator. For nonzero values of Δ we used the tDMRG algorithm and extracted the spectrum of $\rho_A^{T_2}$ following the method described in Ref. 83. In this method all negativities are accessible, and we can use the block structure of the tensor-networks representation for extracting the charge imbalance resolved negativities. However, the dependence of the runtime on the bond dimension is stronger for the extraction of the negativity as compared to the entropy — for bond dimension D the extraction of the entropy requires $O(D^3)$ actions, while the extraction of the negativity requires $O(D^6)$ actions. Thus, we reduced the bond dimension to 256, leading to a truncation error of $\sim 10^{-5}$.

By definition, $\mathcal{N}_{A_1, A_2}^{(1)}(Q)$ is simply the probability distribution of Q . However, it is worthwhile to fit it to the CFT prediction. The reason is that for $n = 1$ we do not apply any twist fields. In this case, our vertex operator 6-point function is just an ordinary free-boson 6-point function, for which the nonuniversal function \mathcal{F} should be equal to unity⁷¹. Fig. 5 presents the fit to Eq. (28) for the XX model for a very large system using the transformation (10), and for the interacting case (using tDMRG) for a finite system using the transformation (12). The fits are seen to work well in the current $n = 1$ case.

The second RN is by definition simply the second RE, or purity, of $A = A_1 \cup A_2$, as mentioned in Ref. 70. We thus skip to the first non-trivial RN, $\mathcal{N}_{A_1, A_2}^{(3)}$. Fig. 6 presents comparisons of the CFT prediction to the ex-

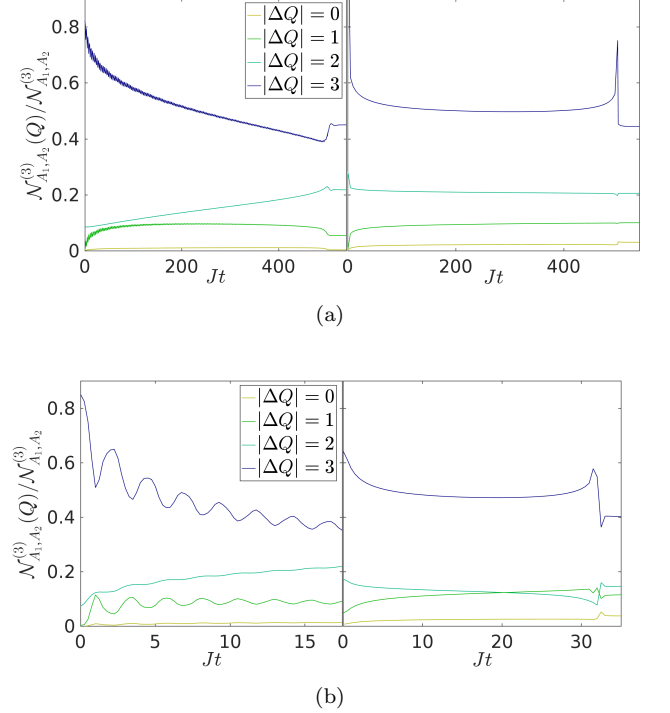


FIG. 6. Comparison between numerical results (left) and CFT predictions (right) for the third imbalance resolved RN. In (a) the XX model results are presented for a large system ($\frac{L}{a} = 10,000$), for $\frac{L}{A_i} = 1000$. (b) Results for the XXZ model with $\Delta = -0.5$, for $\frac{L}{a} = 256$ and $l = \frac{L}{A_i} = 64$.

act ($\Delta = 0$) and tDMRG ($\Delta \neq 0$) results. Here things get complicated: It looks like the function \mathcal{F} modifies some of the qualitative behavior of the prediction as well. We see that while the overall size and trends of the charge-resolved negativities is generally correct for $vt \ll l$, the qualitative behavior is not always fully reproduced. We are left with the conclusion that the effect of the non-universal contribution for the vertex operators 6-point function (imbalance-resolved RNs) has a more pronounced effect than it does for the twist fields 6-point function (total RNs), similarly to the static case⁷².

IV. CONCLUSIONS AND FUTURE OUTLOOK

We expanded the understanding of the charge-resolved entanglement entropies, defined in Ref. 46, and charge-imbalance-resolved entanglement negativities, defined in Ref. 43, by studying for the first time the time-dependence of these quantities following a local quench. We started by analytically calculating the time dependent charge resolved entanglement for 1+1D CFT: We added flux-like vertex operators to the time dependent replica trick following Ref. 46. We then compared the prediction to exact results for the noninteracting XX model, as well as tDMRG results for the critical range

of the XXZ model.

The dependence of the flux-resolved entanglement on the flux appears to be more complicated for smaller systems (whether the entire system is small in size, or just time is short, making the effective length small), and we needed to amend our expression by expanding the vertex operator as in Eq. (19). However, the CFT predictions for the vNEE agrees nicely with the numerical results for Luttinger liquids, both with and without taking the full expansion for the vertex operator.

For the charge imbalance resolved negativity, the time-dependent calculation forced the use of boundary CFT. In this case, high-order correlation functions appear, which are non-universal. General CFT arguments are sufficient for obtaining the qualitative behavior, but the calculation of the full nonuniversal conformal block remains an interesting question for the future.

Our results pave the way towards studying less trivial 1+1D conformal systems, such as those with non-abelian symmetries⁴⁶. It will also be interesting to study the behavior of charge resolved entanglement in non-CFT systems (e.g., topological ones^{84–86}) or conformal systems

of higher dimension. One possible motivation is that the charge-resolved entanglement measures are much more numerically accessible for high values of ΔN_A or ΔQ — these charge or charge imbalance sectors carry less entanglement and hence their corresponding blocks in $\rho_A, \rho_A^{T_2}$ respectively are smaller and easier to diagonalize⁴⁵. Thus, if the expected ΔN_A or ΔQ is known, one can use calculations in these smaller sectors to characterize all sectors.

ACKNOWLEDGMENTS

We would like to thank G. Cohen, E. Cornfeld, E. Grosfeld, and E. Sela for useful discussions. Support by the Israel Science Foundation (Grant No. 227/15), the German Israeli Foundation (Grant No. I-1259-303.10), the US-Israel Binational Science Foundation (Grant No. 2016224), and the Israel Ministry of Science and Technology (Contract No. 3-12419) is gratefully acknowledged.

-
- ¹ A. Einstein, B. Podolsky, and N. Rosen, Phys. Rev. **47**, 777 (1935).
 - ² E. Schrödinger, Die Naturwissenschaften **23**, 807 (1935).
 - ³ M. Srednicki, Phys. Rev. Lett. **71**, 666 (1993).
 - ⁴ S. Ryu and T. Takayanagi, Phys. Rev. Lett. **96**, 181602 (2006).
 - ⁵ P. Calabrese and J. Cardy, Journal of Physics A: Mathematical and Theoretical **42**, 504005 (2009).
 - ⁶ T. Nishioka, S. Ryu, and T. Takayanagi, Journal of Physics A Mathematical General **42**, 504008 (2009).
 - ⁷ L. Amico, R. Fazio, A. Osterloh, and V. Vedral, Rev. Mod. Phys. **80**, 517 (2008).
 - ⁸ R. Horodecki, P. Horodecki, M. Horodecki, and K. Horodecki, Rev. Mod. Phys. **81**, 865 (2009).
 - ⁹ N. Laflorencie, Phys. Rep. **646**, 1 (2016).
 - ¹⁰ A. Osterloh, L. Amico, G. Falci, and R. Fazio, Nature **416**, 608 EP (2002).
 - ¹¹ T. J. Osborne and M. A. Nielsen, Phys. Rev. A **66**, 032110 (2002).
 - ¹² G. Vidal, J. I. Latorre, E. Rico, and A. Kitaev, Phys. Rev. Lett. **90**, 227902 (2003).
 - ¹³ J. I. Cirac and F. Verstraete, Journal of Physics A: Mathematical and Theoretical **42**, 504004 (2009).
 - ¹⁴ F. Verstraete, V. Murg, and J. Cirac, Advances in Physics **57**, 143 (2008).
 - ¹⁵ U. Schollwöck, Annals of Physics **326**, 96 (2011).
 - ¹⁶ R. Orús, Annals of Physics **349**, 117 (2014).
 - ¹⁷ A. K. Ekert, Phys. Rev. Lett. **67**, 661 (1991).
 - ¹⁸ C. H. Bennett and S. J. Wiesner, Phys. Rev. Lett. **69**, 2881 (1992).
 - ¹⁹ C. H. Bennett, G. Brassard, C. Crépeau, R. Jozsa, A. Peres, and W. K. Wootters, Phys. Rev. Lett. **70**, 1895 (1993).
 - ²⁰ P. Shor, SIAM Journal on Computing **26**, 1484 (1997).
 - ²¹ D. Bouwmeester, J.-W. Pan, K. Mattle, M. Eibl, H. Weinfurter, and A. Zeilinger, Nature **390**, 575 (1997).
 - ²² W. K. Wootters, Phys. Rev. Lett. **80**, 2245 (1998).
 - ²³ M. Nielsen and I. Chuang, *Quantum Computation and Quantum Information* (Cambridge University Press, 2000).
 - ²⁴ N. Gisin, G. Ribordy, W. Tittel, and H. Zbinden, Rev. Mod. Phys. **74**, 145 (2002).
 - ²⁵ J. Eisert, *Entanglement in quantum information theory*, Ph.D. thesis (2006).
 - ²⁶ A. W. Harrow, A. Hassidim, and S. Lloyd, Phys. Rev. Lett. **103**, 150502 (2009).
 - ²⁷ J. Von Neumann, *Mathematical Foundations of Quantum Mechanics* (Berlin, Springer, 1932).
 - ²⁸ M. M. Wilde, *From Classical to Quantum Shannon Theory* (Cambridge University Press, 2016).
 - ²⁹ P. Horodecki and A. Ekert, Phys. Rev. Lett. **89**, 127902 (2002).
 - ³⁰ C. Moura Alves and D. Jaksch, Phys. Rev. Lett. **93**, 110501 (2004).
 - ³¹ A. J. Daley, H. Pichler, J. Schachenmayer, and P. Zoller, Phys. Rev. Lett. **109**, 020505 (2012).
 - ³² D. A. Abanin and E. Demler, Phys. Rev. Lett. **109**, 020504 (2012).
 - ³³ H. Pichler, L. Bonnes, A. J. Daley, A. M. Luchli, and P. Zoller, New Journal of Physics **15**, 063003 (2013).
 - ³⁴ R. Islam, R. Ma, P. M. Preiss, M. Eric Tai, A. Lukin, M. Rispoli, and M. Greiner, Nature **528**, 77 EP (2015).
 - ³⁵ L. Banchi, A. Bayat, and S. Bose, Phys. Rev. B **94**, 241117 (2016).
 - ³⁶ A. Elben, B. Vermersch, M. Dalmonte, J. I. Cirac, and P. Zoller, Phys. Rev. Lett. **120**, 050406 (2018).
 - ³⁷ B. Vermersch, A. Elben, M. Dalmonte, J. I. Cirac, and P. Zoller, Phys. Rev. A **97**, 023604 (2018).
 - ³⁸ N. M. Linke, S. Johri, C. Figgatt, K. A. Landsman, A. Y. Matsuura, and C. Monroe, Phys. Rev. A **98**, 052334 (2018).

- (2018).
- ³⁹ T. Brydges, A. Elben, P. Jurcevic, B. Vermersch, C. Maier, B. P. Lanyon, P. Zoller, R. Blatt, and C. F. Roos, *Science* **364**, 260 (2019).
 - ⁴⁰ E. Cornfeld, E. Sela, and M. Goldstein, (2018), arXiv:1808.04471 [cond-mat.stat-mech].
 - ⁴¹ H. Pichler, G. Zhu, A. Seif, P. Zoller, and M. Hafezi, *Phys. Rev. X* **6**, 041033 (2016).
 - ⁴² A. Peres, *Phys. Rev. Lett.* **77**, 1413 (1996).
 - ⁴³ E. Cornfeld, M. Goldstein, and E. Sela, *Phys. Rev. A* **98** (2018), 10.1103/PhysRevA.98.032302.
 - ⁴⁴ J. Gray, L. Banchi, A. Bayat, and S. Bose, *Phys. Rev. Lett.* **121**, 150503 (2018).
 - ⁴⁵ N. Laflorencie and S. Rachel, *Journal of Statistical Mechanics: Theory and Experiment* **11**, P11013 (2014).
 - ⁴⁶ M. Goldstein and E. Sela, *Phys. Rev. Lett.* **120**, 200602 (2018).
 - ⁴⁷ J. C. Xavier, F. C. Alcaraz, and G. Sierra, *Phys. Rev. B* **98**, 041106 (2018).
 - ⁴⁸ H. Barghathi, C. M. Herdman, and A. Del Maestro, *Phys. Rev. Lett.* **121**, 150501 (2018).
 - ⁴⁹ H. Barghathi, E. Casiano-Diaz, and A. Del Maestro, (2019), arXiv:1905.03312 [quant-ph].
 - ⁵⁰ I. Klich and L. Levitov, *Phys. Rev. Lett.* **102**, 100502 (2009).
 - ⁵¹ B. Hsu, E. Grosfeld, and E. Fradkin, *Phys. Rev. B* **80**, 235412 (2009).
 - ⁵² H. F. Song, S. Rachel, and K. Le Hur, *Phys. Rev. B* **82**, 012405 (2010).
 - ⁵³ H. F. Song, C. Flindt, S. Rachel, I. Klich, and K. Le Hur, *Phys. Rev. B* **83**, 161408 (2011).
 - ⁵⁴ H. F. Song, N. Laflorencie, S. Rachel, and K. Le Hur, *Phys. Rev. B* **83**, 224410 (2011).
 - ⁵⁵ H. F. Song, S. Rachel, C. Flindt, I. Klich, N. Laflorencie, and K. Le Hur, *Phys. Rev. B* **85**, 035409 (2012).
 - ⁵⁶ P. Calabrese, M. Mintchev, and E. Vicari, *EPL (Europhysics Letters)* **98**, 20003 (2012).
 - ⁵⁷ E. Vicari, *Phys. Rev. A* **85**, 062104 (2012).
 - ⁵⁸ V. Eisler and Z. Rácz, *Phys. Rev. Lett.* **110**, 060602 (2013).
 - ⁵⁹ V. Eisler, *Phys. Rev. Lett.* **111**, 080402 (2013).
 - ⁶⁰ C.-C. Chien, M. Di Ventura, and M. Zwolak, *Phys. Rev. A* **90**, 023624 (2014).
 - ⁶¹ A. Petrescu, H. F. Song, S. Rachel, Z. Ristivojevic, C. Flindt, N. Laflorencie, I. Klich, N. Regnault, and K. L. Hur, *Journal of Statistical Mechanics: Theory and Experiment* **2014**, P10005 (2014).
 - ⁶² K. H. Thomas and C. Flindt, *Phys. Rev. B* **91**, 125406 (2015).
 - ⁶³ D. Dasenbrook and C. Flindt, *Phys. Rev. B* **92**, 161412 (2015).
 - ⁶⁴ N. A. Sinitsyn and Y. V. Pershin, *Reports on Progress in Physics* **79**, 106501 (2016).
 - ⁶⁵ J. Cardy, (2004), hep-th/0411189.
 - ⁶⁶ J.-M. Stéphan and J. Dubail, *Journal of Statistical Mechanics: Theory and Experiment* **8**, 08019 (2011).
 - ⁶⁷ J. von Delft and H. Schoeller, *Annalen der Physik* **7**, 225 (1998).
 - ⁶⁸ D. Sénéchal, (1999), arXiv:cond-mat/9908262 [cond-mat.str-el].
 - ⁶⁹ P. Calabrese and F. H. L. Essler, *Journal of Statistical Mechanics: Theory and Experiment* **8**, 08029 (2010).
 - ⁷⁰ P. Calabrese, J. Cardy, and E. Tonni, *Journal of Statistical Mechanics: Theory and Experiment* **2013**, 02008 (2013).
 - ⁷¹ P. Francesco, P. Mathieu, and D. Sénéchal, *Conformal Field Theory* (Springer, 1997).
 - ⁷² X. Wen, P.-Y. Chang, and S. Ryu, *Phys. Rev. B* **92**, 075109 (2015).
 - ⁷³ P. Jordan and E. Wigner, *Zeitschrift für Physik* **47**, 631 (1928).
 - ⁷⁴ T. Giamarchi, *Quantum Physics in One Dimension* (Oxford University Press, 2003).
 - ⁷⁵ I. Peschel, *Journal of Physics A: Mathematical and General* **36**, L205 (2003).
 - ⁷⁶ G. Vidal, *Phys. Rev. Lett.* **91**, 147902 (2003).
 - ⁷⁷ G. Vidal, *Phys. Rev. Lett.* **93**, 040502 (2004).
 - ⁷⁸ A. J. Daley, C. Kollath, U. Schollwöck, and G. Vidal, *Journal of Statistical Mechanics: Theory and Experiment* **2004**, 04005 (2004).
 - ⁷⁹ S. R. White and A. E. Feiguin, *Phys. Rev. Lett.* **93**, 076401 (2004).
 - ⁸⁰ A. Weichselbaum, *Annals of Physics* **327**, 2972 (2012).
 - ⁸¹ V. Eisler and Z. Zimborás, *New Journal of Physics* **17**, 053048 (2015).
 - ⁸² V. Eisler and Z. Zimborás, *Phys. Rev. B* **93**, 115148 (2016).
 - ⁸³ P. Ruggiero, V. Alba, and P. Calabrese, *Physical Review B* **94**, 035152 (2016).
 - ⁸⁴ A. Kitaev and J. Preskill, *Phys. Rev. Lett.* **96**, 110404 (2006).
 - ⁸⁵ M. Levin and X.-G. Wen, *Phys. Rev. Lett.* **96**, 110405 (2006).
 - ⁸⁶ E. Cornfeld, L. A. Landau, K. Shtengel, and E. Sela, *Phys. Rev. B* **99**, 115429 (2019).